On the impacting dynamics of ferrofluid droplets on porous substrates in the presence of magnetic field ⊘

Kang-Yang Zeng (曾康扬) ⓘ ; Ya-Ping Wang (王娅萍) ⓘ ; Tian-Pei He (贺天沛) ⓘ ; Zi-Yi Cai (蔡子轶) ⓘ ;
Zhi-Hui Wang (王智慧); Jia-Qing Li (李嘉晴); Xiao-Dong Niu (牛小东) ✉ ⓘ ; Ming-Fu Wen (温明富) ⓘ ;
Mu-Feng Chen (陈木凤); De-Cai Li (李德才); Hiroshi Yamaguchi (山口博司) ⓘ

Check for updates

View Online   Export Citation   CrossMark

Articles You May Be Interested In

Wetting dynamics of a sessile ferrofluid droplet on solid substrates with different wettabilities

Physics of Fluids (April 2021)

Magnetic field based actuation and amalgamation of ferrofluid droplets on hydrophobic surface: An experimental and numerical study

Physics of Fluids (November 2020)

A numerical investigation on the deformation of ferrofluid droplets

Physics of Fluids (January 2023)

On the impacting dynamics of ferrofluid droplets on porous substrates in the presence of magnetic field

View Online · Export Citation · CrossMark

Kang-Yang Zeng (曾康扬),[1,2] Ya-Ping Wang (王娅萍),[1,2] Tian-Pei He (贺天沛),[1,2] Zi-Yi Cai (蔡子轶),[1,2]
Zhi-Hui Wang (王智慧),[1,2] Jia-Qing Li (李嘉晴),[1,2] Xiao-Dong Niu (牛小东),[1,2,a] Ming-Fu Wen (温明富),[1,2]
Mu-Feng Chen (陈木凤),[3] De-Cai Li (李德才),[4] and Hiroshi Yamaguchi (山口博司)[5]

AFFILIATIONS

[1] Key Laboratory of Intelligent Manufacturing Technology, Ministry of Education, Shantou University, 243 Daxue Road,
Shantou 515063, Guangdong, China
[2] College of Engineering, Shantou University, 243 Daxue Road, Shantou 515063, Guangdong, China
[3] College of Physics and Electromechanics Engineering, Longyan University, Longyan 364012, China
[4] Department of Mechanical Engineering, Tsinghua University, Beijing, China
[5] Energy Conversion Research Center, Doshisha University, Kyoto 630-0321, Japan

[a] Author to whom correspondence should be addressed: xdniu@stu.edu.cn

ABSTRACT

This article presents experimental and theoretical studies of the impacting behavior of ferrofluid droplets on porous substrates under the influence of magnetic fields. The effects of magnetic field strength and porous substrates on the falling, impacting, and spreading of the droplets are investigated. Theoretical models are successfully derived to predict the droplet impacting velocity in the presence of the magnetic field and the maximum spreading factor of the droplets on the porous substrates without considering magnetic field effects, respectively. Moreover, a universal scaling law is constructed for the maximum spreading factor of the ferrofluid droplets on both of the porous and smooth substrates in the presence of the magnetic field. The findings of this study can provide a foundation for understanding the impacting dynamics of ferrofluid droplets on the substrates and optimizing their applications in various fields, such as three-dimensional printing and microfluidic technology.

I. INTRODUCTION

The impacting of liquid droplets on porous substrates is an often observed phenomenon in nature,[1] and its controlling and manipulation are crucial in many applications such as herbicide and insecticide in agriculture,[2,3] droplet control in inkjet and liquid three-dimensional (3D) printing,[4] spray cooling and coating of surfaces,[5,6] and forensic research.[7] Despite these wide-range applications, a fully understand of the impacting dynamics of the droplets on the porous substrates is still in a preliminary stage due to the irregular pore structures and external interferences such as electric field[8] or magnetic field[9] complicating the impacting dynamics.

The impacting dynamics of liquid droplets on solid substrates (Fig. 1) is usually governed by a balance between kinetic energy, capillary energy, and viscous dissipation and is mainly controlled by contact angle θ, and dimensionless parameters of impact Reynolds number

$Re = \rho V_0 D_0/\eta$, Weber number $We = \rho V_0^2 D_0/\gamma$, Bond number $B_o = \rho g D_0^2/\gamma$, and Ohnesorge number $Oh = \eta/\sqrt{\rho D_0 \gamma} = \sqrt{We}/Re$, where D_0 and V_0 are the initial drop diameter and impact velocity, and ρ, η, γ, and g are the liquid density, viscosity, surface tension, and gravitational acceleration, respectively. One of the most important parameters relevant to the droplet impacting mentioned earlier is the maximum spreading diameter D_{max}, which is often normalized to the original diameter of the droplet prior to impact and defined by a dimensionless form $\beta_{max} = D_{max}/D_0$. So far, various theoretical correlations have been proposed in the literature to predict β_{max},[10] which is generally described with acceptable accuracy in two regimes dominated by capillary force and viscous dissipation, respectively. In the viscous regime, it is found that β_{max} follows the law of $Re^{1/5}$,[11] while in the capillary regime, a law of $\beta_{max} \propto We^{1/2}$ is observed.[12] A general approximation[7] can be formulated with interpolation approach
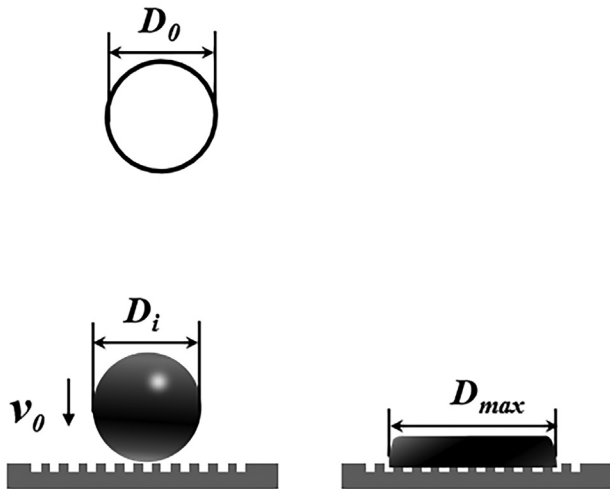
FIG. 1. Schematic diagram of magnetic fluid droplet impacting a solid porous substrate.

between $e^{1/5}$ and $We^{1/2}$ to connect the viscous and capillary regimes as $\beta_{max} \propto Re^{1/5} f(P)$ with $f(P) = P^{1/2}/A + P^{1/2}$, where $P = WeRe^{-2/5}$ and A is a fitting constant. The above correlation is further improved by considering the effect of the contact angle.[13]

Despite an abundance of theoretical approaches in this area, theoretical models for predicting the droplet impact on the porous substrates in the presence of the external interferences are few in the literature. Most recent studies are focusing application aspects and dynamic contact angle of droplets on the porous substrates such as mass loading of droplet printing on sieve substrates,[14] bioinspired programmable wettability arrays for droplets manipulation,[15] and substrate roughness affecting the dynamic contact angle.[16,17] In this work, we present a study of a ferrofluid droplet impacting on porous substrates under the action of magnetic fields. Ferrofluid is a stable colloidal suspension with surfactant-coated ferro-nanoparticles dispersed in carrier fluids like water or oil, and it exhibits both the fluidity of a liquid and superparamagnetic properties when immersed in an applied magnetic field.[18] Understanding the impact dynamics of the ferrofluid droplets on the porous substrates is also crucial for modern burgeoning applications such as digital electronics[19] and 3D printing industries.[4]

In the most recent studies, Zhang *et al.*[20] developed a theoretical model with numerical validation and demonstrated that the maximum spreading ratio of a metal droplet under the influence of the magnetic field can be scaled by the ratio of the magnetic force to the inertial force. Li *et al.*[21] systematically investigated the maximum spreading of ferrofluid droplets impacting on a smooth hydrophobic surface under the non-uniform magnetic fields and developed a generalized model for scaling the maximum spreading factor. To the best of our knowledge, the above two works are the only available theoretical models that discuss the drop impact dynamics in the presence of a magnetic field but lack consideration of porous substrates.

The main objective of the present work is to experimentally and theoretically study the dynamics of a ferrofluid droplet impacting on the porous substrates in the presence of the magnetic fields, and develop a scaling law for the maximum spreading factor of the ferrofluid droplet with considerations of the effects of the magnetic field and the porous structure of the substrates. To find a scaling law of the maximum spreading factor for the impacting ferrofluid droplet on the porous substrates, a generalized theoretical model is derived based on energy balance theory, and a universal scaling relation is obtained by introducing a dimensionless magnetic parameter $N_m = \rho V_0^2 / \mu_0 \chi H^2$, where $\mu_0 = 4\pi \times 10^{-7}$ is vacuum magnetic permeability, χ and H are magnetic susceptibility and magnetic field intensity, respectively, and a correction coefficient for porous effects, and this relation allows us to rescale all experimental data of the present work and Li *et al.*[21] onto a single curve with the Padé approximant,[7] which is highly applicable in a wide range of impact velocities and magnetic field strengths.

II. MATERIALS AND METHOD
A. Ferrofluid and porous substrates

The ferrofluid used in this work is a water-based ferrofluid with a volume concentration of 9%–13% and PH value of 9–10 (The EMG series, Ferrotec). The saturation magnetization M_s and initial magnetic susceptibility χ of the ferrofluid are 200 Gs and 0.6, respectively, while the density and viscosity of that fluid are $1.18 \times 10^3 \, \text{kg/m}^3$ and 5 mPa s, respectively. The surface tension of the ferrofluid is found to be 26 mN/m.

Three different porous substrates are printed by a high-precision photosensitive resin 3D printers (QZ Experiment, Hangzhou) and have a rectangular shape with uniformly square-pore distributions. The pore sizes on the substrates have height of 100 μm and length of 60, 70, and 80 μm, respectively. The equilibrium contact angle θ of the water-based ferrofluid on them is 39.306°, 55.316°, and 76.864° (SDC-350, Dongguan Shengding Precision Instrument Co., Ltd.), respectively, in the absence of the magnetic field.

B. Experimental setup

The schematic diagram of the experimental setup is sketched in Fig. 2, where an electromagnet is placed below the solid substrate with a DC power source. The intensity of the magnetic field can be increased or decreased by adjusting the input current. The porous substrates are placed above the electromagnet, and a Gauss meter (KANETEC, TM-801) is used to measure the specific magnetic induction intensity (B) of the droplets at different heights from the center of the electromagnet. A matching software in an automatic tilting contact angle measuring instrument (SDC-350, Dongguan Shengding Precision Instrument Co., Ltd.) is used to control the volume and height of the ferrofluid droplets through a syringe pump with a flat-tipped needle. The same device can also measure the contact angle of the spreading droplet. To capture the temporal evolution and impacting dynamics of the droplet, a high-speed camera (Fast Cam Mini AX200 PHOTRON LIMI TED) is used.

C. Experiment

In experiment, the droplet impacting platform is first placed in a suitable position so that the droplet motion is clearly visualized on the computer screen, and a scaled image is taken and saved as a reference for pixel value calibration. The ferrofluid droplet is generated by a syringe pump with a flat-tipped needle. The droplet volume is fixed at
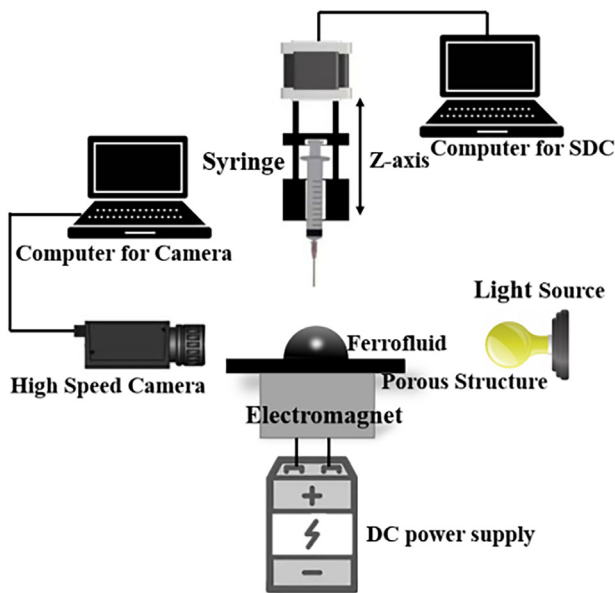
FIG. 2. Schematic diagram of experimental apparatus.

5 μL, and its corresponding approximated diameter is $D_0 = 2.12$ mm. The droplet dynamics is recorded by setting the camera at 3000 fps with a resolution of 1024 × 1024. The impacting velocity of the falling droplet is varied by varying the height of the needle above the substrate. A custom-made image processing MATLAB code is used to calculate the droplet impact diameter D_i, impact velocity V_0, and maximum spreading diameter D_{max}.

The magnetic induction intensity of the electromagnet is controlled by adjusting the DC power, and three gradient magnetic fields with magnetic induction intensities of $B_0 = 16$, 24, and 32 mT are set in experiment, respectively. Figure 3 shows the magnetic field distributions in z direction along the centerline of the electromagnet. The center of the upper surface of the electromagnet is chosen as the origin of the coordinates, and the magnetic field strength at height $z_0 = 0$ is defined as B_0. The solid symbols in Fig. 3 are the measured values, while the dotted lines are the fitting curves. The magnetic induction
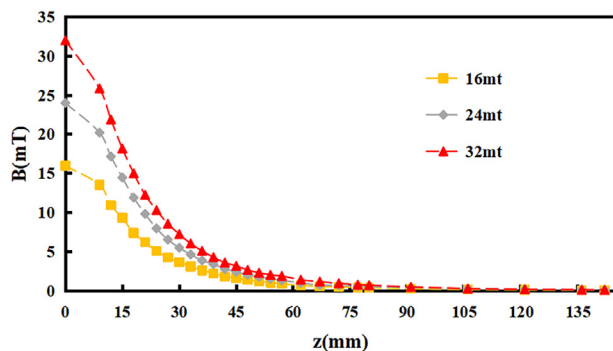

FIG. 3. The variation of magnetic induction intensity along the Z axis at the center of the electromagnetic coil.

intensities are measured three times at each position along the z axis, and the three-time data are averaged to obtain the relationship between the height and the magnetic flux density.

III. RESULTS AND DISCUSSION

The motion of a ferrofluid droplet in the presence of the magnetic field undergoes a combined action of drag force from the surrounding air, magnetic Kelvin force $F_{mg} = \mu M \cdot \nabla H$ (μ is magnetic permeability, H is magnetic field intensity, and M is magnetization), gravitational force F_g, and surface tension F_s of the droplet, and follows the following momentum equation:[9]

$$\frac{\partial \rho u}{\partial t} + \nabla(\rho u u) = -\nabla p + \nabla \cdot \left[\eta \left(\nabla u + (\nabla u)^T \right) \right] F_s + F_g + F_{mg},$$

(1)

where p is the pressure, u denotes the velocity, t is the local time, and η is the dynamic viscosity. However, for convenience, the theoretical analyses for the subsequent experimental results presented are built on the bases of energy balance, which can be directly derived from the above equation.

A. Deformation of the ferrofluid droplet during the falling process

A liquid droplet falling in air in the presence of the magnetic field demonstrates shape oscillation. Figure 4 shows the shape deformation of the falling ferrofluid droplets under different magnetic fields [Fig. 4(a)] and the variation of the short-axis diameter D of the droplets with time t in second. As shown in Fig. 4(a), when the ferrofluid droplet detaches from needle, the leading end of the droplet is affected by a transient tension at the neck (rear end of the droplet),[21] which increases the droplet curvature [Fig. 4(b)]. As shown in Fig. 4(b), the applied magnetic field reduces the oscillation frequency while increases the oscillated amplitude of the droplet shape, which reaches an elliptic shape in the end.

B. Impacting velocity of the ferrofluid droplet

Before colliding with the substrates, the impacting velocity of the falling ferrofluid droplet can theoretically be derived based on the law of energy conservation. Assuming the droplet to be a rigid ellipsoidal sphere before its colliding, the motion of the droplet follows,[21]

$$E_{k0} + E_{s0} = E_g + E_m,$$

(2)

where E_g and E_m are the respective gravitational potential energy and magnetic energy of the droplet after it just leaving from the needle, and E_{k0} and E_{s0} are the droplet kinetic energy and surface energy, respectively, before impacting. The expressions for each energy are as follows:[21]

$$E_g = mgh = \rho \Omega gh,$$

(3)

$$E_m = \mu_0 MH = \frac{\chi B^2}{\mu_0 (1+\chi)^2} \Omega,$$

(4)

$$E_{s0} = \left[2\pi b^2 + \left(\frac{ab}{e} \right) \arcsin(e) \right] \gamma,$$

(5)

where $M = \chi H$ and $B = \mu_0(M + H) = \mu_0(1+\chi)H$ are magnetization strength and magnetic induction strength, respectively; Ω and h
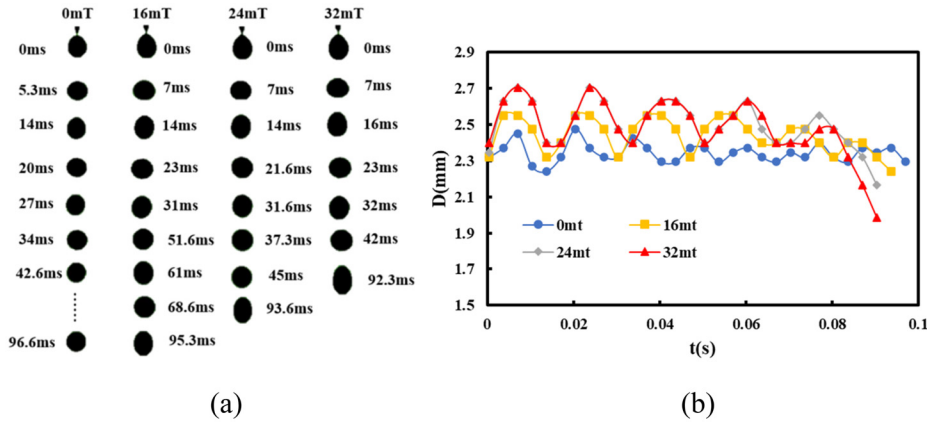
FIG. 4. (a) Shape deformation of the falling ferrofluid droplets under different magnetic fields; and (b) variation of the short-axis diameter of the falling ferrofluid droplets with time.

(a) 　　　　　　　　　　　　　　(b)

are the droplet volume and initial height, respectively; a and b are the half lengths of the respective long and short axes of the droplet, and $e = \sqrt{1 - \frac{b^2}{a^2}}$ is the eccentricity of the droplet.

If a magnetic material is uniformly magnetized in an applied magnetic field, the internal demagnetization field H_d generated by itself is proportional to the magnetization strength M of the material, that is,

$$H_d = -NM, \tag{6}$$

where N is a demagnetization factor with its value related to the geometry of the material.[22] With the above consideration, the magnetic energy E_m can be further expressed as

$$E_m = \frac{\chi B^2}{\mu_0(1 + N\chi)}\Omega. \tag{7}$$

Based on Eqs. (2)–(7), the theoretical impacting velocity of the ferrofluid droplet on the substrates is derived as

$$V_0 = \sqrt{2gh + \frac{2\chi(B_2{}^2 - B_1{}^2)}{\rho\mu_0(1 + N\chi)} - \frac{2\gamma\left[2\pi b^2 + \left(\dfrac{ab}{e}\right)\arcsin(e)\right]}{\rho\Omega}}, \tag{8}$$

where B_1 and B_2 are the magnetic inductions at the positions of the needle tip and the substrate surface.

Figure 5 presents a comparison of the measured impacting velocities and those calculated from Eq. (6) for the droplet falling from different heights. It can be observed that the droplet impacting velocity increases with the height, and at the same height, the droplet impacting velocity increases with the magnetic field strength. The theoretical values calculated from Eq. (6) are consistent with the experimental data. Figure 6 illustrates the relationship between the impacting Reynolds number and the impacting Weber number, calculated from the experimental data and theoretical calculations shown in Fig. 5. Clearly, all the data follow the law of $Re = 51We^{1/2}$, which can be used to analysis the spreading dynamics of the ferrodroplet after it impacting on the substrates in Subsections III C and III D.
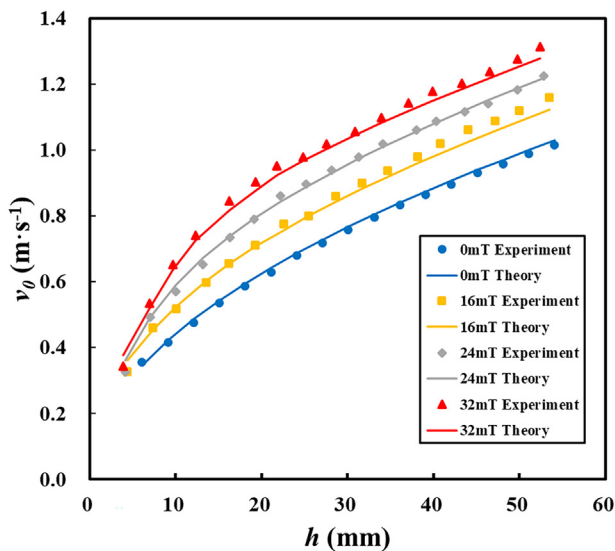
C. Maximum spreading of the ferrofluid droplet on the porous substrates in the absence of magnetic field

The maximum spreading of a droplet on a solid surface is also estimated based on the energy balance theory.[21] Assuming the droplet prior to the impact be a sphere and the total drop surface energy
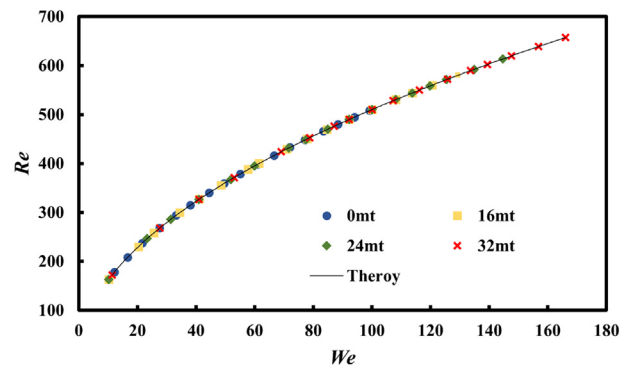

FIG. 5. The impacting velocities of the droplet varying with the needle height at different magnetic fields.

FIG. 6. The impacting Reynolds number varies the impacting Weber number.

consisting of only the liquid–vapor interfacial tension γ. Thus, immediately before the impact the total considered energy in the system includes the kinetic energy and the surface energy of the droplet. To obtain the maximum spreading ratio of the non-magnetized ferrofluid droplets, the corresponding energy equation can be written as follows:[21]

$$E_{k0} + E_{s0} = E_k + E_s + W_{vis} + W_{cl}, \tag{9}$$

where E_k, E_s, W_{vis}, and W_{cl} are the kinetic energy, surface energy, work done due to viscous dissipation, and moving contact line dissipation, respectively, at the maximum spreading of the droplet on the substrates. Since the kinetic energy is completely converted to surface energy and dissipation at maximum spreading, $E_k = 0$. The expressions for other energies are given as follows:[21]

$$E_{k0} = \frac{\pi}{12} \rho V_0^2 D_0^3, \tag{10}$$

$$E_{s0} = \pi D_0^2 \gamma, \tag{11}$$

$$W_{vis} = \int_0^{t_{max}} \int_\Omega \Phi d\Omega dt \approx \Phi \Omega t_{max}, \tag{12}$$

where t_{max} is the time of the droplet to spread its maximum and Φ is the viscous dissipation function. According to the theory proposed by Lee et al.,[13] $t_{max} = c \frac{D_{max}}{V_0}$, where c is the ratio of the surface tension of the test liquid droplet to that of the reference fluid (water). As the porous structures of the substrates also affect the spreading time, a value of $c = \frac{1}{2}$ is used in the present analyses. Thus, the maximum spreading time can be represented as (Fig. 7)

$$t_{max} = \frac{1}{2} \frac{D_{max}}{V_0}. \tag{13}$$

The magnitude Φ and the volume of the droplet are estimated with the help of the radial velocity and characteristic size of the droplet,[23,24] and they are given by $\Phi \approx \mu \left(\frac{V_0}{\delta} \right)^2$ and $\Omega = \frac{\pi D_{max}^2 \delta}{4}$, respectively, with $\delta = 2 \frac{D_0}{\sqrt{Re}}$. With Eq. (12) and the above estimations, the viscous dissipation becomes
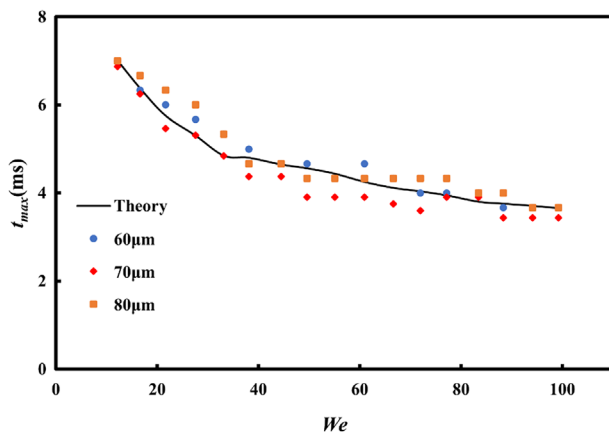
$$W_{vis} = \frac{\pi}{16} \frac{\rho V_0^2 D_{max}^3}{\sqrt{Re}}. \tag{14}$$

For the surface energy, based on an assumption of the droplet be a cylindrical shape at the maximum spreading stage,[25] it can be expressed as

$$E_s = \frac{\pi}{4} (1 - \varphi \cos \theta) \gamma D_{max}^2 + \frac{2\pi \gamma D_0^2}{3 D_{max}} \tag{15}$$

with

$$\varphi = 1 + \left(\frac{2h_r}{D_r + D_p} \right) \left(\frac{1 - \cos \alpha}{\sin \alpha} \right). \tag{16}$$

Here, φ, h_r, D_r, and D_p are the roughness factor, pore depth, pore diameter, and pore spacing distance of the porous substrates, respectively; $\alpha = 90°$ is the side angle of the cylindrical pore column.

Based on the study of Vaikuntanathan and Sivakumar on the impact dynamics of liquid droplets on dual-textured surfaces,[26] when the droplet connects the two different parts of the surface during impact, the contact line dissipation can be expressed as

$$W_{cl} = \frac{\pi}{4(D_r + D_p)} \gamma (\cos \theta - \cos \theta_a) D_{max}^3, \tag{17}$$

where θ_α represents the advancing contact angle. Considering Eqs. (9)–(17), the maximum spreading factor $\beta_0 = D_{max}/D_0$ in the absence of the magnetic field is formulated as

$$\left[\frac{3}{4} \frac{We}{\sqrt{Re}} + \frac{3D_0}{D_r + D_p} (\cos \theta - \cos \theta_a) \right] \beta_0^4$$
$$+ 3(1 - \varphi \cos \theta) \beta_0^3 - (We + 12) \beta_0 + 8 = 0. \tag{18}$$

Figure 8 shows the maximum spreading factors varying with the Weber number, and the data of the non-magnetized ferrofluid droplets impacting on a polydimethylsiloxane (PDMS) smooth substrate[21] are also included. The roughness factors for the three porous substrates of 60, 70, and 80 μm are 2.67, 2.43, and 2.25, respectively. As there are
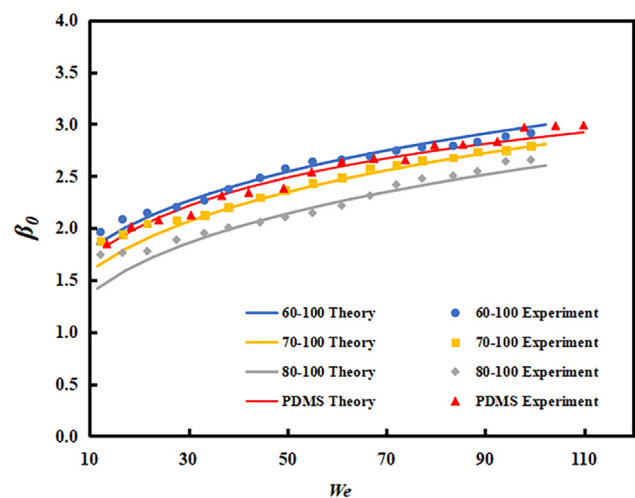

FIG. 7. Comparison between the theoretical and measured maximum spreading time t_{max} varying with We.

FIG. 8. Variation of the maximum spreading factor β_0 with We.

usually a penetration of the droplet into the porous substrates to form a "liquid slug" due to the capillary effects, a spontaneous dissipation related to "interface relaxation" during droplet spreading, and a surface depression of the droplet when the maximum spreading achieved,[1,6,7,27] the theoretical maximum spreading factor β_0 for the porous substrates is corrected based on the experimental data by multiplying a factor of 1.4 and a factor of 1.25 for the smooth substrates, respectively, to eliminate the above effects. As shown in Fig. 8, with the Weber number increasing, the maximum spreading factor increases; the smaller the pore size of the substrates, the larger the maximum spreading factor. After correction, the theoretical values are generally well agreed with the experimental data. In addition, it is concluded that the behavior of water-based ferrofluid droplets impacting on both porous and smooth substrate in the absence of magnetic field is the same as that of a water droplet, and both Eq. (18) and the present experimental data flows the scaling law Re $\propto$ We$^{1/4}$ for the maximum spreading factor.

D. A universal scaling law for the maximum spreading of the ferrofluid droplet on the porous substrates in the presence of magnetic field

In the presence of the magnetic field, the maximum spreading factor is defined as $\beta_{max} = \frac{D_{max}}{D_i}$, where D_i is the actual diameter of the ferrofluid droplet before impact (Fig. 1). Figure 9 shows the shapes of the ferrofluid droplets before impact (a) and the maximum spreading shapes of the ferrofluid droplets after impact (b) on the porous substrates and at different magnetic fields. Figure 10 plots the maximum spreading factor β_{max} varying with We with pore size (a) 60, (b) 70, and (c) 80 μm, respectively. As shown these two figures, D_i is decreased with the increasing magnetic field [Fig. 9(a)], and for all the test porous substrates, the maximum spreading factor β_{max} increases with increasing the Weber number, but decreases with the pore size increasing (Fig. 10). However, Fig. 10 demonstrates the maximum spreading factor β_{max} irregularly varies with increasing magnetic field.

When a magnetic field is applied, the droplet is magnetized under the action of the Kelvin force, which is expressed as

$$f_k = \mu_0 M \nabla H = \frac{\mu_0 M \partial H}{\partial z}. \tag{19}$$

According to Josserand and Zaleski[28] and Eggers, et al.[29] the droplet spreading time follows $t \sim D_i/V_0$, so the acceleration of the droplet under the Kelvin force can be approximated by

$$\frac{Dv}{Dt} = \frac{\mu_0 M \partial H}{\rho \partial z}. \tag{20}$$

As $Dv/Dt \sim v_0^2/D_i$ and $\partial H/\partial z \sim H/D_i$, we can have the dimensionless magnetic parameter N_m, and

$$N_m^{-1} = \frac{\mu_0 \chi H^2}{\rho V_0^2}, \tag{21}$$

where N_m is the ratio of the inertial force to the Kelvin force. Assuming the Kelvin force and heat dissipation can be offset in a short period of time, and all kinetic and magnetic energies are converted into the thermal energy,[21] we have

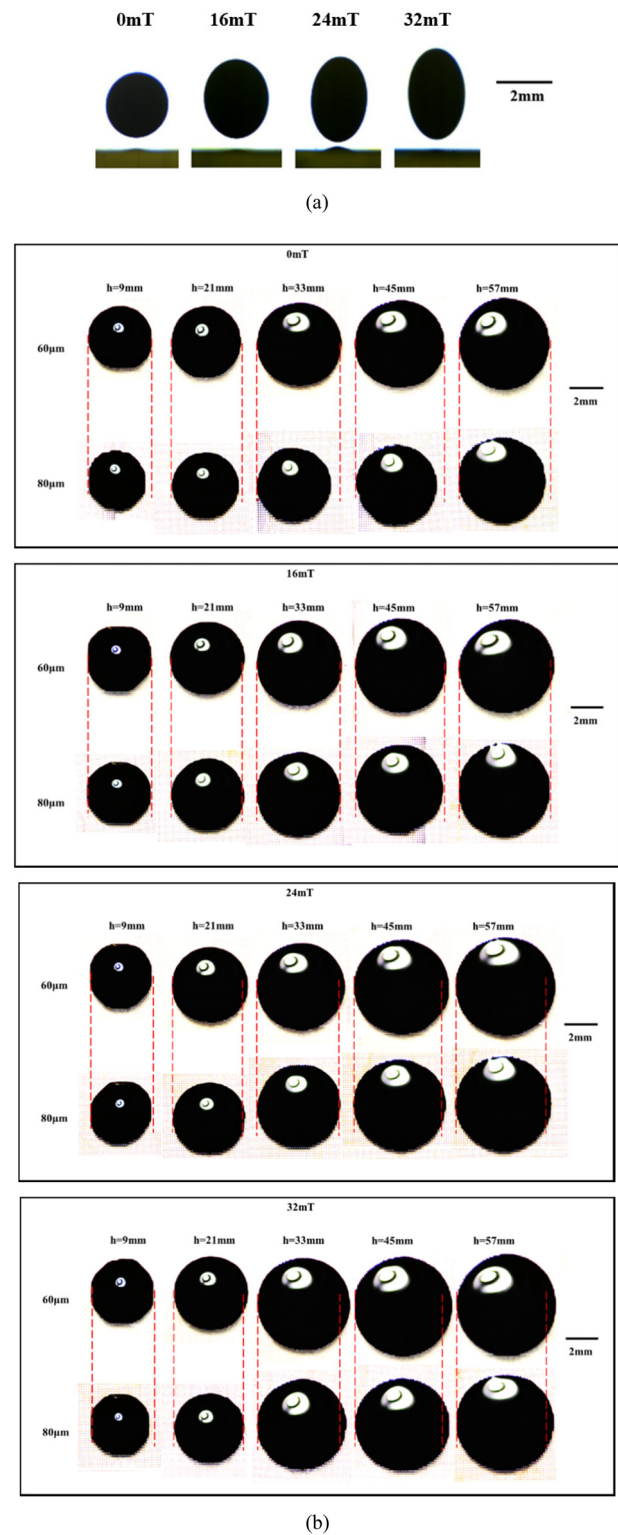$$\rho V_0^2 D_0^3 \sim \mu_0 \chi H^2 \beta_{max} D_0^3, \tag{22}$$

(a)

(b)

FIG. 9. (a) Shapes of the ferrofluid droplets before impacting (side view). (b) Maximum spreading D_{max} on porous surfaces with different heights (top view).
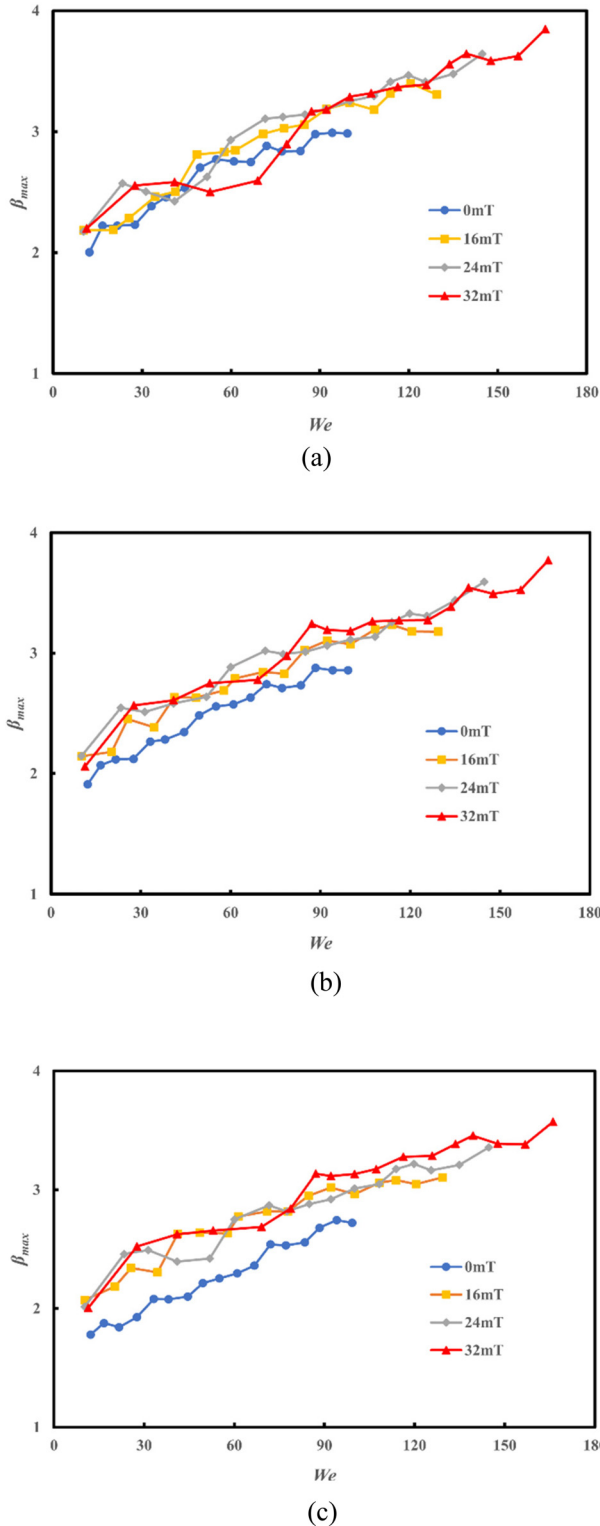
(a)

(b)

(c)

FIG. 10. Variation of the maximum spreading factor β_{max} with We on different porous substrates with pore size (a) 60, (b) 70, and (c) 80 μm.
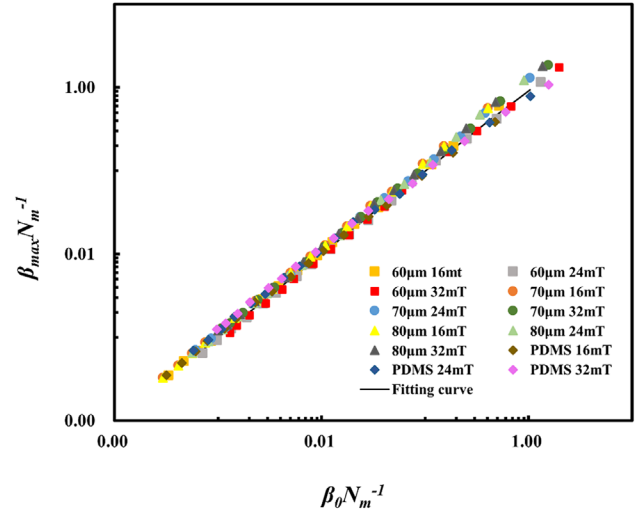

FIG. 11. The rescaled maximum spreading ratio as a function of P, with the solid line showing the interpolating function Eq. (20) fitted to the experimental results.

which can be further formulated by a scalar rate of $\beta_{max}N_m^{-1}$, and β_{max} can be expressed as a function of $\beta_{max}N_m^{-1}$ as[7,21]

$$\beta_{max} \sim N_m f_{EC}(\beta_0 N_m^{-1}), \tag{23}$$

where f_{EC} is a univariate scaling function of $\beta_0 N_m^{-1}$. By defining $P = \beta_0 N_m^{-1}$, we finally have

$$\beta_{max}N_m^{-1} = P/(1 + AP), \tag{24}$$

where $A = 0.1$ is the fitting constant obtained by least squares fitting, and $f_{EC}(P)$ satisfies $lim_{P\to 0}\beta_{max} = \beta_0$ and $lim_{P\to\infty}\beta_{max} = N_m$. Actually, Eq. (23) is the Padé approximation,[7,29] which is used to construct a smooth crossover between two asymptotic points.

According to Fig. 11, the falling spreading of magnetic droplets under different porous substrates can be seen, and the data of Li et al.[21] on the falling spreading of ferromagnetic droplets on PDMS membranes under gradient magnetic field are also introduced. As can be seen from the figure, the theoretical prediction by Eq. (24) are in good agreement with the present experimental values, all experimental data on the porous and PDMS substrates fall on the theoretical line. It can be concluded from these data that the spreading morphology of ferrofluid droplets under different substrates follows a universal scaling law of Eq. (24).

IV. CONCLUSIONS

In this work, the impacting dynamics of the ferrofluid droplet on the porous substrates in the presence of the magnetic field are investigated experimentally and theoretically.

First, we find that, compared to that of no magnetic field applied, the ferrofluid droplet undergoes more severe shape oscillation during its falling under the effect of the magnetic fields. Additionally, we have derived a theoretical model that considers the effects of magnetic fields, and the model can provide precise predictions of the impacting velocity of the ferrofluid droplets as well as the variation of the impacting Reynolds number with the Weber number.

Second, the theoretical model for the maximum spreading of the droplet on the porous substrates without the presence of the magnetic field is also formulated, and it shows good consistency with the present experimental data. It has also revealed that the maximum droplet spreading has a proportional relationship with the Weber number. This study has created an opportunity to address some unanswered issues regarding industrial applications, such as maximizing the drop-to-drop contact area and adhesion during 3D printing.

Finally, a key insight into the maximum spreading dynamics of the ferrofluid droplet impacting on the porous and smooth substrates in the presence of the magnetic field can be scaled to a single line with the scaling law of $\beta_{max} \sim N_m f_{EC}(\beta_0 N_m^{-1})$, and this is of great importance in developing manipulation techniques for droplets.

AUTHOR DECLARATIONS
Conflict of Interest

The authors report no conflict of interest.

Author Contributions

Kang-Yang Zeng: Data curation (equal); Formal analysis (equal); Investigation (equal); Methodology (equal); Software (equal); Writing – original draft (equal). **De-Cai Li:** Investigation (equal); Resources (supporting). **Hiroshi Yamaguchi:** Investigation (equal); Visualization (equal). **Ya-Ping Wang:** Data curation (equal); Formal analysis (equal); Methodology (equal); Software (equal). **Tian-Pei He:** Data curation (equal); Formal analysis (equal); Methodology (equal); Software (equal). **Zi-Yi Cai:** Data curation (equal); Formal analysis (equal). **Zhi-Hui Wang:** Data curation (equal); Formal analysis (equal). **Jia-Qing Li:** Data curation (equal); Formal analysis (equal). **Xiao-Dong Niu:** Conceptualization (equal); Data curation (equal); Formal analysis (equal); Funding acquisition (equal); Methodology (equal); Supervision (equal); Writing – review & editing (equal). **Ming-Fu Wen:** Funding acquisition (equal); Writing – review & editing (equal). **Mu-Feng Chen:** Investigation (equal); Methodology (equal).

DATA AVAILABILITY

The data that support the finding of this study are available from the corresponding author upon reasonable request.

REFERENCES

[1] A. L. Yarin, "Drop impact dynamics: Splashing, spreading, receding, bouncing…," Annu. Rev. Fluid Mech. **38**, 159–192 (2006).

[2] V. Bergeron, D. Bonn, J. Y. Martin, and L. Vovelle, "Controlling droplet deposition with polymer additives," Nature **405**(6788), 772–775 (2000).

[3] S. El-Sapa and A. Almoneef, "The axisymmetric migration of an aerosol particle embedded in a Brinkmann medium of a couple stress fluid with slip regime," Eur. J. Pure Appl. Math. **15**(4), 1566–1592 (2022).

[4] C. W. Visser, R. Pohl, C. Sun, G.-W. Römer, B. Huis in 't Veld, and D. Lohse, "Toward 3D printing of pure metals by laser-induced forward transfer," Adv. Mater. **27**(27), 4087–4092 (2015).

[5] J. Kim, "Spray cooling heat transfer: The state of the art," Int. J. Heat Fluid Flow **28**(4), 753–767 (2007).

[6] V. M. Starov and M. G. Velarde, *Wetting and Spreading Dynamics* (CRC Press, 2019), Vol. 12.

[7] N. Laan, K. G. de Bruin, D. Bartolo, C. Josserand, and D. Bonn, "Maximum diameter of impacting liquid droplets," Phys. Rev. Appl. **2**(4), 044018 (2014).

[8] O. Ghazian, K. Adamiak, and G. S. P. Castle, "Spreading and retraction control of charged dielectric droplets," Colloids Surf., A **448**, 23–33 (2014).

[9] S. El-Sapa, "Effect of magnetic field on a microstretch fluid drop embedded in an unbounded another microstretch fluid," Eur. J. Mech.-B **85**, 169–180 (2021).

[10] M. Pasandideh-Fard, Y. M. Qiao, S. Chandra, and J. Mostaghimi, "Capillary effects during droplet impact on a solid surface," Phys. Fluids **8**(3), 650–659 (1996).

[11] I. V. Roisman, R. Rioboo, and C. Tropea, "Normal impact of a liquid drop on a dry surface: Model for spreading and receding," Proc. R. Soc. London, Ser. A **458**, 1411–1430 (2002).

[12] C. Ukiwe and D. Y. Kwok, "On the maximum spreading diameter of impacting droplets on well-prepared solid surfaces," Langmuir **21**(2), 666–673 (2005).

[13] J. B. Lee, N. Laan, K. G. de Bruin, G. Skantzaris, N. Shahidzadeh, D. Derome, J. Carmeliet, and D. Bonn, "Universal rescaling of drop impact on smooth and rough surfaces," J. Fluid Mech. **786**, R4 (2016).

[14] C. D. Modak, A. Kumar, A. Tripathy *et al.*, "Drop impact printing," Nat. Commun. **11**, 4327 (2020).

[15] L. Sun, F. Bian, Y. Wang, Y. Wang, X. Zhang, and Y. Zhao, "Bio-inspired programmable wettability arrays for droplets manipulation," Proc. Natl. Acad. Sci. U. S. A. **117**, 4527–4532 (2020).

[16] K. Sarah and H. Ulrich, "Contact angle measurement on porous substrates: Effect of liquid absorption and drop size," Colloids Surf., A **619**, 126503 (2021).

[17] X. Chen, G. Wen, and Z. Guo, "What are the design principles, from the choice of lubricants and structures to the preparation method, for a stable slippery lubricant-infused porous surface?," Mater. Horiz. **7**(7), 1697–1726 (2020).

[18] R. E. Rosensweig, "Directions in ferrohydrodynamics," J. Appl. Phys. **57**(8), 4259–4264 (1985).

[19] G. Katsikis, J. S. Cybulski, and M. Prakash, "Synchronous universal droplet logic and control," Nat. Phys. **11**(7), 588–596 (2015).

[20] J. Zhang, T.-Y. Han, J.-C. Yang, and M.-J. Ni, "On the spreading of impacting drops under the influence of a vertical magnetic field," J. Fluid Mech. **809**, R3 (2016).

[21] Q.-P. Li, Y. Ouyang, X.-D. Niu, Y. Jiang, M.-F. Wen, Z.-Q. Li, M.-F. Chen, D.-C. Li, and H. Yamaguchi, "Maximum spreading of impacting ferrofluid droplets under the effect of nonuniform magnetic field," Langmuir **38**(8), 2601–2607 (2022).

[22] E. C. Stoner, "XCVII. The demagnetizing factors for ellipsoids," London, Edinburgh Dublin Philos. Mag. J. Sci. **36**(263), 803–821 (1945).

[23] S. Chandra and C. T. Avedisian, "On the collision of a droplet with a solid surface," Proc. R. Soc. London, Ser. A **432**(1884), 13–41 (1991).

[24] F. H. Harlow and J. P. Shannon, "The splash of a liquid drop," J. Appl. Phys. **38**(10), 3855–3866 (1967).

[25] Y. Yonemoto and T. Kunugi, "Analytical consideration of liquid droplet impingement on solid surfaces," Sci. Rep. **7**(1), 2362 (2017).

[26] V. Vaikuntanathan and D. Sivakumar, "Directional motion of impacting drops on dual-textured surfaces," Phys. Rev. E **86**(3), 036315 (2012).

[27] G. Zhang, M. A. Quetzeri-Santiago, C. A. Stone, L. Botto, and J. R. Castrejón-Pita, "Droplet impact dynamics on textiles," Soft Matter **14**(40), 8182–8190 (2018).

[28] C. Josserand and S. Zaleski, "Droplet splashing on a thin liquid film," Phys. Fluids **15**(6), 1650–1657 (2003).

[29] J. Eggers, M. A. Fontelos, C. Josserand, and S. Zaleski, "Drop dynamics after impact on a solid wall: Theory and simulations," Phys. Fluids **22**(6), 062101 (2010).